

Increasing the Efficiency of the Power Electronic Converter for a Proposed Dual Stator Winding Squirrel-Cage Induction Motor Drive Using a Five-Leg Inverter at Low Speeds

H. Moayedirad, M. A. Shamsi Nejad *

Faculty of Electrical and Computer Engineering, University of Brjand, Birjand, Iran.

Abstract- A dual stator winding squirrel-cage induction motor (DSWIM) is a brushless single-frame induction motor that contains a stator with two isolated three-phase windings wound with dissimilar numbers of poles. Each stator winding is fed by an independent three-phase inverter. The appropriate efficiency of this motor is obtained when the ratio of two frequencies feeding the machine is equal to the ratio of the number of poles. In the vector control method at low speeds, flux is difficult to estimate because the voltage drop on the stator resistance is comparable with the input stator voltage, disturbing the performance of the motor drive. To solve the abovementioned problem, researchers have benefited from the free capacity of the two windings of the stator. This makes the motor deviate from its standard operating mode at low speeds. The main purpose of this paper is reducing the power losses of the inverter unit in the DSWIM drive at low speeds via the proposed control method and a five-leg inverter. This paper deals with two topics: 1. Using the idea of rotor flux compensation at low speeds, the motor works in its standard operating mode. Therefore, the power losses of the utilized power electronic converters are also reduced to a considerable extent; and 2. Reduction in capital cost can be achieved by utilizing a five-leg power electronic converter. The proposed methods are simulated in MATLAB/Simulink software, and the results of simulation confirm the assumptions.

Keyword: Dual stator winding, Five-leg inverter, Induction machine, Low speed, Vector control.

1. INTRODUCTION

Induction machines have a wide range of application in industry, for example, in pumps, fans, compressors, roller mills for cement, mining elevators, and motive force of ships and vehicles [1]. AC induction motors, and especially the squirrel-cage types, are the most common machines used in AC drive systems with adjustable speeds. Nowadays, more than 70 % of motors used in industries are induction motors [2]. By optimizing their utilization, a considerable percentage of electrical energy consumed by them can be saved.

With regard to the interesting performance of the induction motor and its wide usage, in recent years, researchers have improved the characteristics of this motor by adding another balanced three-phase winding on its stator. In fact, the doubly-fed (excited) induction motor is a brushless induction motor that has a stator

with two separate symmetric three-phase windings wound with dissimilar numbers of poles. The doubly-fed induction machine can be classified into brushed and brushless categories. The brushed machine has a wound rotor, and the ends of windings are connected to slip rings which are mounted on the shaft such that these ends can be accessed through the brushes. Brushless doubly-fed induction motors usually have two types of rotors, i.e. squirrel-cage and nested loop rotors. These rotors have a higher durability compared to the wound rotor models. For the case of a squirrel-cage rotor, the motor is commonly fed by two three-phase inverters, each of which is connected separately to the grid. The drive of these kinds of machines can control them in a wide range of operating speeds. As a result, doubly-fed machines can be categorized based on the type of stator winding and rotor used, as shown in Fig. 1.

A doubly-fed induction motor with a nested loop rotor is known as a brushless doubly-fed machine. These machines are also consisted of two separate stator windings, one of which is directly connected to the grid and is called the power winding, and the other one is connected to the grid via a three-phase inverter and is called the control winding. This machine works at low speeds and is suitable for drives with a narrow speed

Received: 05 Nov. 2016

Revised: 19 Mar. 2017

Accepted: 27 Aug. 2017

*Corresponding author:

E-mail: mshamsi@birjand.ac.ir (M. A. Shamsi Nejad)

Digital object identifier: 10.22098/joape.2018.2990.1249

© 2018 University of Mohaghegh Ardabili. All rights reserved.

range. Furthermore, this kind of machine is more prevalent as a generator [3,4].

The dual stator winding induction motor (DSWIM) studied in this paper consists of a stator with two separate symmetric three-phase windings with dissimilar numbers of poles and a standard squirrel-cage rotor. This motor was presented by Lipo et al. [5] and has a high degree of reliability. In normal situations, the two three-phase windings of the stator of this motor are connected to the grid via two three-phase inverters. There is no internal electrical connection between the two windings of the stator. In this motor, circulating harmonic currents are eliminated by using different numbers of poles in stator windings. A DSWIM acts like two independent three-phase induction machines which share a common shaft [5].

Generally, the poles of the stator are chosen in the ratio of 1 to 3 (e.g. 2:6 or 4:12). However, any combination of different pole numbers can be selected. Additionally, these ratios are recommended for the better use of magnetic material, avoiding saturation, and reducing stator losses [5].

The standard operating mode of a DSWIM is obtained when the ratio of two frequencies feeding the machine is equal to the ratio of the number of poles. The two resulting rotating fields rotate synchronously. Consequently, this operating mode leads to the proper performance of the motor. The required condition for the motor to have the maximum value of torque per ampere ratio (T/I) is working in its standard operating mode [6].

Each stator winding is fed by an independent inverter through a common DC-bus. Fig. 2(a) shows a simple schematic diagram of a DSWIM drive.

Adjusting the speed of the induction motor is one of the most important needs of industries and automation of factories. The speed control of doubly-fed induction motors is complicated because of their multi-variable and nonlinear structure. By developing and improving power electronic devices, the implementation of advanced control methods has become possible.

A DSWIM is similar to two independent three-phase induction motors that are mechanically coupled. Therefore, speed control methods used for three-phase induction motors are also applicable to the DSWIM [5,6]. All known control techniques utilized in induction motors consist of scalar control methods [5,7], the direct torque control (DTC) [8-10] and the vector control [11-18].

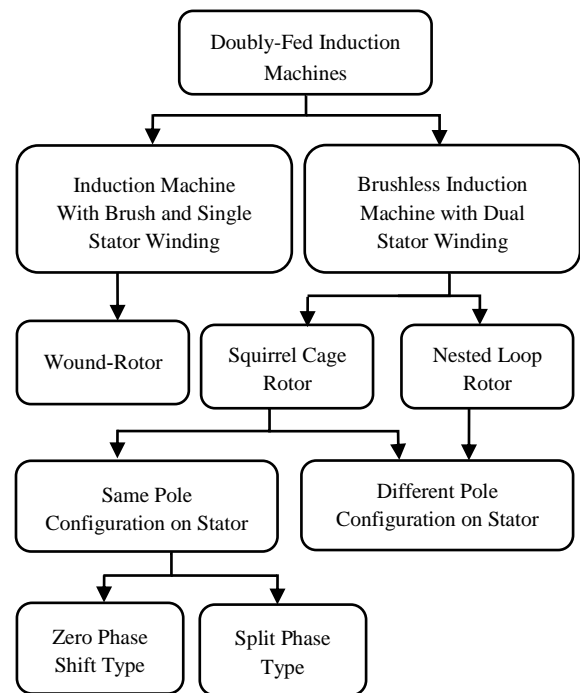


Fig. 1. Classification of doubly-fed induction machines according to the arrangement of stator winding and rotor type.

The most common method of speed control in induction motors is vector control [14,15]. The vector control method is one of the most powerful controlling techniques for induction motor drives which, compared to scalar methods, has a high accuracy and less dependency on motor parameters [17]. This control method depends on flux estimation [16]. Here, unlike the scalar control method, flux and torque can be controlled distinctly. Moreover, amplitude and phase are controlled simultaneously. The torque and flux in the air-gap are functions of voltage and frequency. This dependence is the main reason for the slow response of induction motors. Using the vector control method can improve the slowness of response. In this method, at low speeds, the estimation of flux has noticeable sensitivity and error because the voltage drop on the stator resistance is comparable to the input stator voltage, thus disturbing the performance of the motordrive. Therefore, at low speeds, an appropriate level of rotor flux is very important.

Based on conventional control methods, the DSWIM drive in its standard operating mode cannot properly trace low speeds. One of the features of DSWIM is that it has two separate stator windings. Until now, researchers have benefited from this hardware feature of DSWIM for solving the typical problem of speed control at low speeds. In the method proposed in [5], one of the windings is fed by an arbitrary constant

frequency (usually 0.05 p.u.) and the other one is fed by a variable frequency. This operating mode forces the low-pole winding to produce a torque larger than that of the load. In other words, unlike the first winding, the second one can produce negative and positive torques dependent upon the desired speed and torque. Consequently, by enforcing the first winding to work at an arbitrary constant frequency, the two rotating fields produced by the windings rotate asynchronously and the motor deviates from its standard operating mode, but the problem of drive for tracing low speeds is solved.

The vector control methods presented in [11,12] are based on the seminal method presented by [5]. The torque produced by the windings of the stator is divided between them in such a way that either the first winding or the second one will be able to produce a negative or positive torque at low speeds. The conventional control method leads to the loss of optimal energy management at low speeds in DSWIM. The proper efficiency of this motor is obtained when it works in its standard operating mode [6].

The adaptive control model based on torque function presented in [19] cannot be used at low speeds due to voltage drop on the stator resistance. In [20], for high speeds, the flux approaches saturation due to the large value of electromotive force. In [21-24], the stator resistance estimation has been utilized at a low speed range to solve the problem of the speed control of motor. In [25], artificial intelligent has been employed for improving the performance of the speed control drive of the induction motor, resulting in an improvement in the steady-state response of the drive. However, this method has not been successful in solving the problem of the drive at low speeds. In [26-28], different kinds of reformed extended Kalman filter (EKF) algorithms are presented for improving flux and torque estimation. EKF is a suitable algorithm for estimation, processed based on algorithm repetition. Due to the high complexity, computation time is long. In [29], an induction motor flux estimation method is proposed based on a new integration method with a closed loop DC offset compensation algorithm. This method estimates an exact flux only when the system parameters are known.

In [16], a rotor flux compensator has been used to improve the time response and the problem of estimating the rotor flux of a three-phase induction motor drive at a low speed range. This has perfectly solved the problem of rotor flux estimation at low speeds without estimating stator resistance.

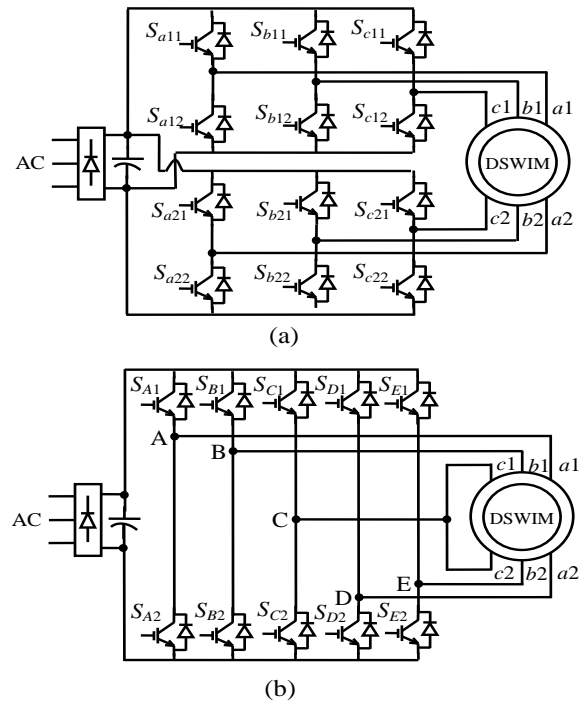


Fig. 2. Schematic diagram of DSWIM drive with: a) Two three-phase inverters, and b) The proposed five-leg inverter.

In all the presented methods of DSWIM drive, two distinct three-phase inverters are utilized, making a total of 12 switches (see Fig. 2(a)). Reducing the number of power electronic switching devices can reduce the cost [30, 31]. Implementing a five-leg (ten-switch) inverter for separately controlling two three-phase induction motors was investigated in [30,32-35], and the results confirmed the possibility of the fully independent control of the two motors. The schematic diagram of a five-leg inverter for a DSWIM drive is demonstrated in Fig. 2(b).

In this paper, a vector control method is first presented based on the rotor flux compensation method, and the performance of DSWIM drive is studied in standard operating mode at a low speed range. Afterwards, a five-leg inverter is implemented in the proposed DSWIM drive. The main purpose of this paper is reducing the power losses of the inverter unit in the DSWIM drive at low speeds via the proposed control method and a five-leg inverter.

The paper is organized as follows: A model of squirrel-cage induction motor with two windings is presented in Sec. 2. The proposed vector control for the DSWIM drive based on two three-phase inverters and the model used for rotor flux compensation are explained in Sec. 3. In Sec. 4, the five-leg inverter is studied. In Sec. 5, the calculation of power losses in the inverter is explained. Simulation results are given in

Sec. 6, and finally, the conclusion is presented in Sec. 7.

2. MACHINE MODEL

The d-q equations of the voltage signal in a dual stator winding induction motor with different numbers of poles can be expressed in complex form as Eqs. (1) and (2) [5].

$$V_{qdsi} = r_{si} i_{qdsi} + \rho \lambda_{qdsi} - j\omega \lambda_{qdsi} \quad (1)$$

$$V_{qdri} = r_{ri} i_{qdri} + \rho \lambda_{qdri} - j(\omega - \omega_{ri}) \lambda_{qdri} = 0 \quad (2)$$

where i can be 1 or 2, presenting the parameters and state variables of each three-phase stator winding ($abc1$ and $abc2$). ω is the electrical rotating speed of the common reference frame and ω_{ri} is the rotor electrical speed. V_{qdsi} and V_{qdri} are stator q - and d -axis voltages. i_{qdsi} and i_{qdri} are stator q - and d -axis currents. λ_{qdsi} and λ_{qdri} are stator q - and d -axis flux linkages. r_{si} and r_{ri} are stator and rotor resistances, and $\rho = d/dt$.

Flux linkage equations given in terms of currents are provided by Eq. (3) [36].

$$\begin{bmatrix} \lambda_{qdsi} \\ \lambda_{qdri} \end{bmatrix} = \begin{bmatrix} L_{si} & L_{mi} \\ L_{mi} & L_{ri} \end{bmatrix} \times \begin{bmatrix} i_{qdsi} \\ i_{qdri} \end{bmatrix} \quad (3)$$

where L_{mi} is the magnetizing inductance, and L_{ri} and L_{si} are rotor and stator inductances. From Eq. (3), stator and rotor currents can be expressed in terms of flux linkages as Eqs. (4) and (5).

$$i_{qdsi} = \frac{L_{ri}}{D_i} \lambda_{qdri} - \frac{L_{mi}}{D_i} \lambda_{qdri} \quad (4)$$

$$i_{qdri} = \frac{L_{si}}{D_i} \lambda_{qdri} - \frac{L_{mi}}{D_i} \lambda_{qdsi} \quad (5)$$

where $D_i = L_{si} L_{ri} - L_{mi}^2$. Substituting Eq. (4) into Eq. (1) and also Eq. (5) into Eq. (2), the voltage equations become Eqs. (6) and (7).

$$V_{qdsi} = \frac{r_{si} L_{ri}}{D_i} \lambda_{qdsi} - \frac{r_{si} L_{mi}}{D_i} \lambda_{qdri} + p \lambda_{qdsi} - j\omega \lambda_{qdsi} \quad (6)$$

$$0 = \frac{r_{ri} L_{si}}{D_i} \lambda_{qdsi} - \frac{r_{ri} L_{mi}}{D_i} \lambda_{qdri} + p \lambda_{qdri} - j(\omega - \omega_{ri}) \lambda_{qdri} \quad (7)$$

The electromagnetic torque (T_{ei}) for each stator winding is given in complex variable form by Eq. (8).

$$T_{ei} = \frac{3}{2} \frac{P_i}{2} \text{Im}(\lambda_{qdsi} i_{dqsi}^*) \quad (8)$$

where P_i is the pole number for windings, $i=1$ or 2. The total electromagnetic torque (T_e) of a DSWIM is the sum of produced torques via both stator windings, which is given as Eq. (9) [5].

$$T_e = T_{e1} + T_{e2} = \frac{3}{2} \frac{P_1}{2} \text{Im}(\lambda_{qds1} i_{dqsl}^*) + \frac{3}{2} \frac{P_2}{2} \text{Im}(\lambda_{qds2} i_{dqsl}^*) \quad (9)$$

Rotor electrical speeds ω_{r1} and ω_{r2} can be defined in terms of the rotor mechanical speed (ω_r) as Eqs. (10) and (11) [12]. The air-gap flux linkage is expressed as Eq. (12).

$$\omega_{r1} = \frac{P_1}{2} \omega_r \quad (10)$$

$$\omega_{r2} = \frac{P_2}{2} \omega_r \quad (11)$$

$$\lambda_{qdm} = L_{mi} i_{qdsi} + L_{mi} i_{qdri} \quad (12)$$

The currents are eliminated by substituting Eqs. (4) and (5) into Eq. (12). Therefore, the air-gap flux linkage of each stator winding can be stated in terms of rotor and stator flux linkages, as Eq. (13).

$$\lambda_{qdm} = \frac{L_{lr1} L_{mi}}{D_i} \lambda_{qdsi} + \frac{L_{ls1} L_{mi}}{D_i} \lambda_{qdri} \quad (13)$$

The total air-gap flux linkage is the sum of the two separate air-gap flux linkages, which is defined as Eq. (14).

$$\lambda_{qdm} = \frac{L_{lr1} L_{m1}}{D_1} \lambda_{qds1} + \frac{L_{ls1} L_{m1}}{D_1} \lambda_{qdri1} + \frac{L_{lr2} L_{m2}}{D_2} \lambda_{qds2} + \frac{L_{ls2} L_{m2}}{D_2} \lambda_{qdri2} \quad (14)$$

If the total air-gap flux linkage is aligned with the d -axis, then the total air-gap flux linkage on the q -axis and its derivative will always be zero, which is expressed as Eq. (15). Assuming that the leakage flux is constant, the time derivative of the total air-gap flux linkage on the q -axis is given by Eq. (16).

$$\lambda_{qm} = \frac{L_{lr1} L_{m1}}{D_1} \lambda_{qs1} + \frac{L_{ls1} L_{m1}}{D_1} \lambda_{qr1} + \frac{L_{lr2} L_{m2}}{D_2} \lambda_{qs2} + \frac{L_{ls2} L_{m2}}{D_2} \lambda_{qr2} = 0 \quad (15)$$

$$p \lambda_{qm} = \frac{L_{lr1} L_{m1}}{D_1} p \lambda_{qs1} + \frac{L_{ls1} L_{m1}}{D_1} p \lambda_{qr1} + \frac{L_{lr2} L_{m2}}{D_2} p \lambda_{qs2} + \frac{L_{ls2} L_{m2}}{D_2} p \lambda_{qr2} = 0 \quad (16)$$

In addition, the mechanical equation of the machine is explained by Eq. (17).

$$p \omega_r = \frac{K_{e1}}{J} (\lambda_{dr1} I_{qs1} - \lambda_{qr1} I_{ds1}) + \frac{K_{e2}}{J} (\lambda_{dr2} I_{qs2} - \lambda_{qr2} I_{ds2}) - \frac{T_L}{J} \quad (17)$$

where J is the inertia coefficient, $K_{e1}=(3P_1/4)(L_{m1}/L_{r1})$, and $K_{e2}=(3P_2/4)(L_{m2}/L_{r2})$. The equivalent circuit of DSWIM is shown in Fig. 3 using d - q notation [5]. An illustration of the winding distribution with poles in the ratio of 2:6 in a DSWIM is depicted in Fig. 4 [5]. The low-pole number winding is referred to as $abc1$ and the high-pole number winding as $abc2$.

3. THE PROPOSED VECTOR CONTROL OF THE DSWIM DRIVE USING TWO THREE-PHASE INVERTERS

The block diagram of the vector control method for a dual stator winding squirrel-cage induction motor is illustrated in Fig. 5. The fundamentals of vector control structure can be explained in this figure. A machine model with internal conversions is shown on the right. The machine model is presented in a synchronously rotating reference frame. Principal vector control parameters, i_{dsi}^* and i_{qsi}^* , are DC values in the synchronously rotating frame. Unit vectors $\sin\omega_e t$ and $\cos\omega_e t$ are generated by the rotor flux signal.

The d^e - q^e and d^s - q^s axes are demonstrated in the form of phasor diagrams in Fig. 6 for the induction motor [37]. Equations (18)-(28) are utilized for generating feedback signals [5, 37].

$$\varphi_{dsi}^s = \int (v_{dsi}^s - R_{si}i_{dsi}^s) dt \tag{18}$$

$$\varphi_{qsi}^s = \int (v_{qsi}^s - R_{si}i_{qsi}^s) dt \tag{19}$$

$$\varphi_{qdsi}^s = \varphi_{qsi}^s - L_{lsi}i_{qdsi}^s \tag{20}$$

$$\varphi_{dri}^s = (L_{ri} / L_{mi})\varphi_{dmi}^s - L_{lri}i_{dsi}^s \tag{21}$$

$$\varphi_{qri}^s = (L_{ri} / L_{mi})\varphi_{qmi}^s - L_{lri}i_{qsi}^s \tag{22}$$

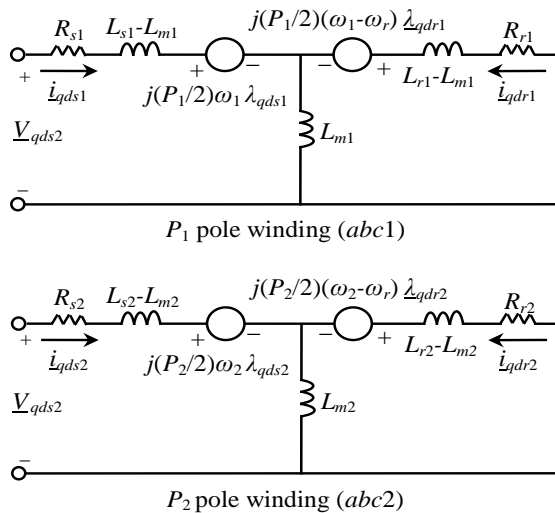


Fig. 3. The equivalent circuit of a dual stator winding squirrel-cage induction motor [5].

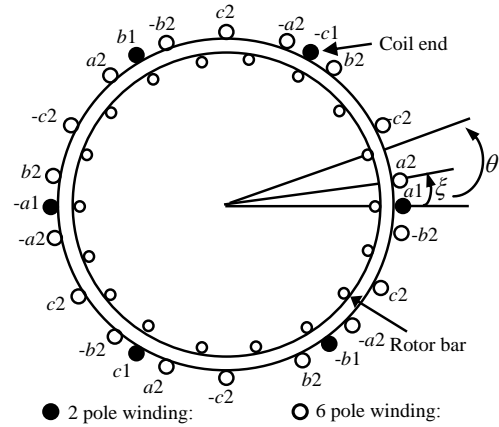


Fig. 4. The winding distribution in DSWIM [5].

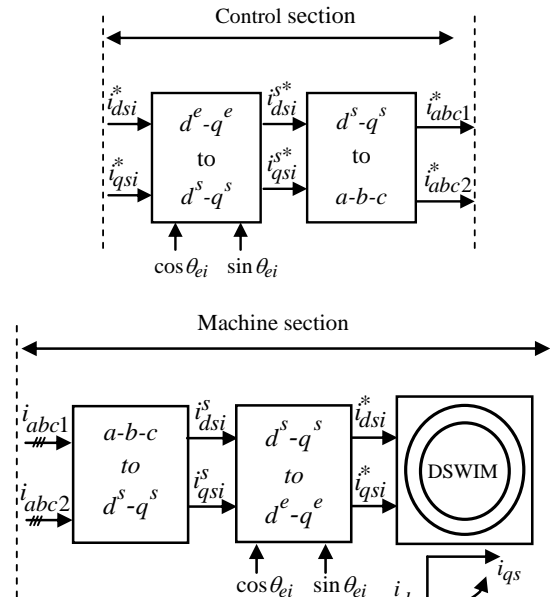


Fig. 5. Block diagram of the vector control method for a dual stator winding squirrel-cage induction motor.

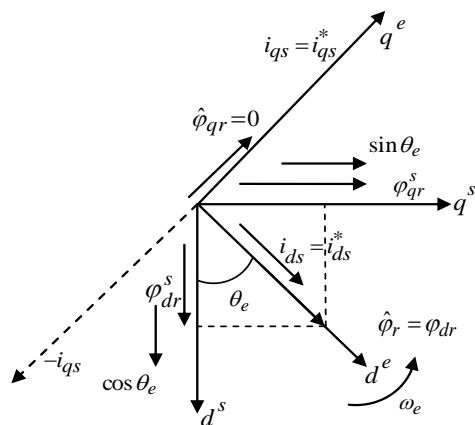


Fig. 6. Phasor diagram of d^e - q^e and d^s - q^s [37].

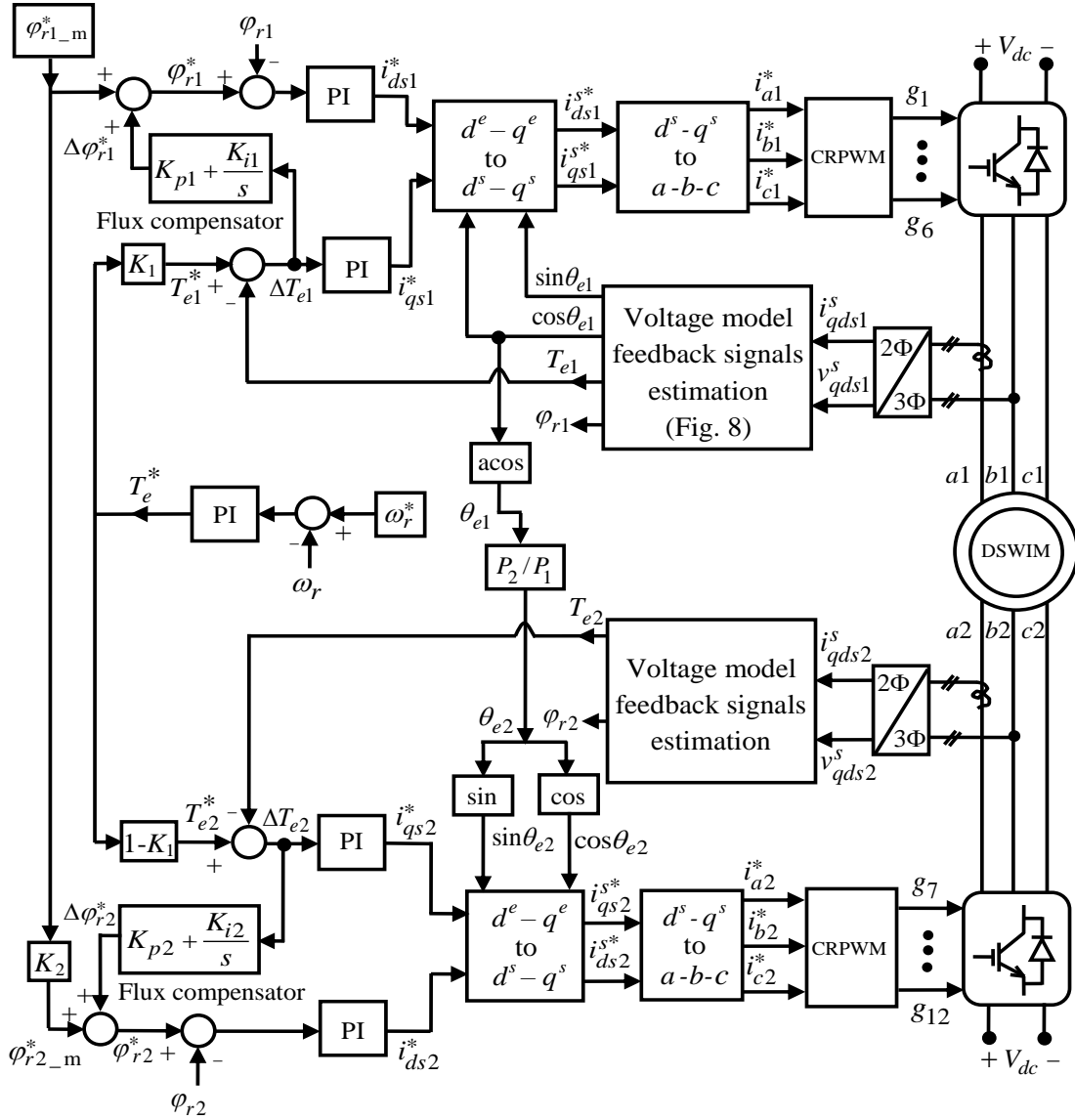


Fig. 7. Block diagram of the proposed control of the DSWIM using two three-phase inverters (12 switches).

$$T_{ei} = (3P_i / 4)(\varphi_{dsi}^s i_{qsi}^s - \varphi_{qsi}^s i_{dsi}^s) \quad (23)$$

$$\varphi_{ri} = \sqrt{(\varphi_{qri}^s)^2 + (\varphi_{dri}^s)^2} \quad (24)$$

$$\cos\theta_{ei} = \varphi_{dri}^s / \varphi_{ri} \quad (25)$$

$$\sin\theta_{ei} = \varphi_{qri}^s / \varphi_{ri} \quad (26)$$

$$\varphi_{dri}^s = L_{mi} i_{dsi}^s + L_{ri} i_{dri}^s \quad (27)$$

$$\varphi_{qri}^s = L_{mi} i_{qsi}^s + L_{ri} i_{qri}^s \quad (28)$$

where φ_{dsi}^s and φ_{qsi}^s are stator q - and d -axis fluxes, respectively; φ_{dri}^s and φ_{qri}^s are rotor q - and d -axis fluxes,

respectively; L_{lsi} and L_{lri} are stator and rotor leakage inductances, respectively; and φ_{dmi}^s and φ_{qmi}^s are q - and d -axis air-gap fluxes, respectively.

The scheme of the DSWIM proposed drive using a direct vector control is shown in Fig. 7 where K_1 and K_2 are the torque-sharing factor and the flux coefficient, respectively.

3.1. Voltage model feedback signal estimation

The direct vector control of the voltage model acts based on the generation of unit vector signals from rotor fluxes. Based on Fig. 8, rotor fluxes can be estimated from the values of air-gap fluxes as Eqs. (21) and (22).

Also, air-gap fluxes (φ_{qm}^s and φ_{dm}^s) can be estimated from the values of voltage and current of the phases. The stator currents of the motor are directly measured by current sensors. Rotor flux, electromagnetic torque, and $\sin\omega_e t$ and $\cos\omega_e t$ signals are estimated from the block diagram in Fig. 8 [37]. Moreover, for the $abc2$ winding, the required signals in the drive control system are estimated as in Fig. 8.

3.2. Flux compensation model

The direct vector control depends on the estimation of unit vectors and rotor flux. The estimated rotor flux is proportional to the difference between the stator voltage and the voltage drop on the stator resistance. At high speeds, due to $V_s \geq R_s i_s$, the rotor flux has less dependence on the voltage drop on the stator resistance. However, at low speeds, the voltage drop on stator resistance is comparable with the input voltage. As a result, the rotor flux cannot be effectively established, which makes the operation of the controller difficult at low speeds. A low flux results in a low induced torque which cannot drive the DSWIM. If torque error always exists ($\Delta T_e \neq 0$), then the actual torque T_e is always less than the reference torque (T_e^*).

A rotor flux compensator is utilized to compensate for these variations [16]. In this compensator, the rotor flux is compensated with a general proportional and integral (PI) controller whose input is the torque error [16]. Rotor flux is compensated when the torque error (ΔT_e) exists. In fact, the main objective of a speed control drive is to reduce the torque error to zero, which in turn reduces the speed error to zero.

At low speeds, the estimated rotor flux ($\hat{\varphi}_{ri}$) is not equal to its actual value φ_{ri} ($\varphi_{ri} \neq \hat{\varphi}_{ri}$). In order to compensate for the main reference flux (φ_{ri}^*), the component of $\Delta\varphi_{ri}^*$ is employed. This component is generated by the flux compensator and adjusts the main reference flux to be $\varphi_{ri}^* = \varphi_{ri,m}^* + \Delta\varphi_{ri}$. This method directly establishes an effective flux without identifying the stator resistance [16].

From Eqs. (18) and (19), the flux in the drive control system of DSWIM is directly obtained by integrating the electromotive force. The pure integrator has the problem of DC offset to solve which the algorithm presented in [38] is utilized. The block diagram of the integration algorithm is shown in Fig. 9.

In the system of the proposed control method for $T_e > 0$, total torque is defined as $T_e = T_{e1} + T_{e2} = |T_{e1}| + |T_{e2}|$, although it is defined as $T_e = T_{e1} + T_{e2} \neq |T_{e1}| + |T_{e2}|$ in the conventional method.

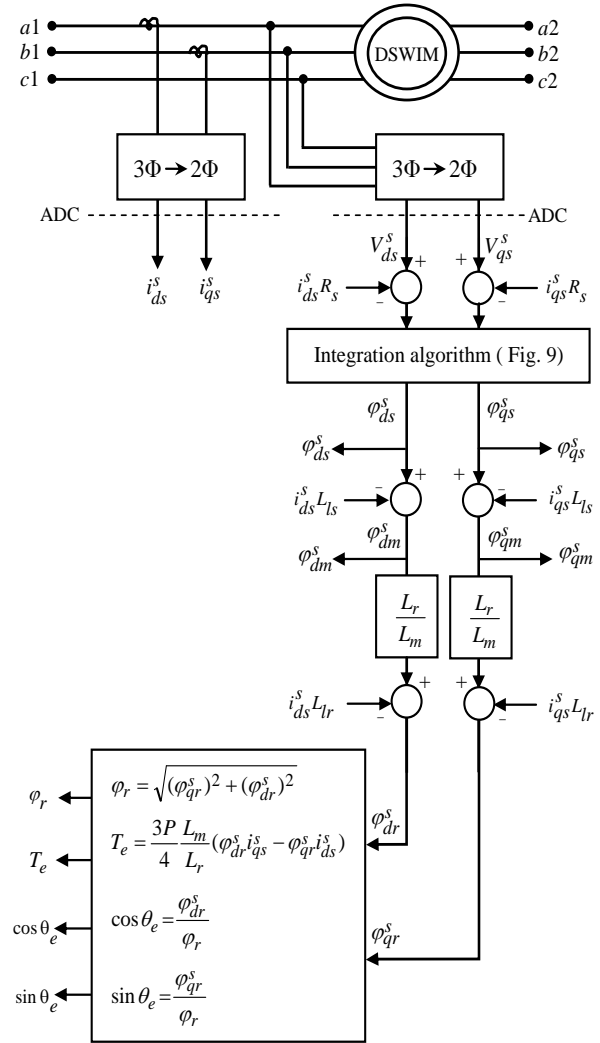


Fig. 8. Block diagram of the estimation of voltage model feedback signals for the DSWIM proposed drive.

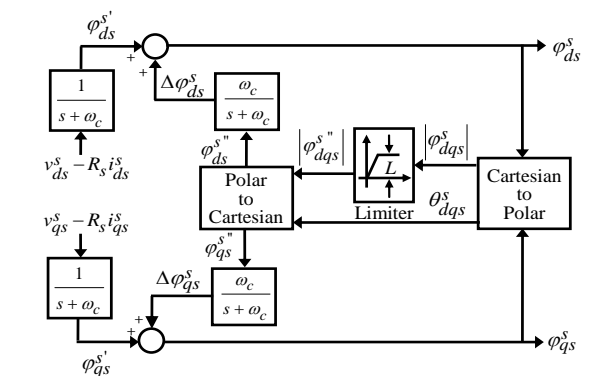


Fig. 9. Block diagram of the integration algorithm for solving the problem of DC offset of the pure integrator in the DSWIM.

4. THE PROPOSED VECTOR CONTROL OF THE DSWIM DRIVE USING A FIVE-LEG INVERTER

The schematic diagram of a DSWIM drive based on a ten-switch inverter is illustrated in Fig. 2(b). A five-leg

inverter needs five modulation signals ($v_j(t)$, $j=A, B, C, D, E$) to generate switching commands.

Three modulation signals exists from each of the three-phase windings, making six modulation signals in total. In [30], a technique is described as in Eq. (29) to reduce the number of signals from six to five.

$$v_i(t) = v_i^*(t) + v_{no}(t) \quad (29)$$

where $v_{no}(t)$ represents the zero-sequence signal, and $i=a, b, c$ and $v_i^*(t)$ are fundamental sinusoidal reference signals. In the technique presented by [30], the modulation signal of the third phase of each winding ($v_{c1}(t)$ and $v_{c2}(t)$) is added to the modulation signals of the other winding phases ($v_k(t)$, $k = a1, b1, a2, b2$), as in Eq. (30). The advantage of the zero-sequence is that it does not appear in line-to-line voltages [30].

$$\begin{aligned} v_A(t) &= v_{a1}(t) + v_{c2}(t), v_B(t) = v_{b1}(t) + v_{c2}(t), \\ v_C(t) &= v_{c1}(t) + v_{c2}(t), v_D(t) = v_{a2}(t) + v_{c1}(t), \\ v_E(t) &= v_{b2}(t) + v_{c1}(t) \end{aligned} \quad (30)$$

5. POWER LOSSES IN THE INVERTER

Inverters have the main role in controlling electrical systems such as industrial drives [39]. At low speeds, the loss of the motor core is not significant [40]. Therefore, minimizing the power losses of the inverter unit with the lowest cost is important for a higher energy efficiency.

Insulated-gate bipolar transistors (IGBT) are the most utilized elements of an electromotive inverter unit. The reliability of IGBTs depends on the heat management of the utilized elements. Thus, taking account of power losses of the inverter unit has a great importance in increasing the operational efficiency and reliability of the inverter unit.

The losses of IGBT/Diode consist of two parts, i.e. IGBT losses and diode losses. Each part can be further divided into commutation losses (P_{sw}) and conduction losses (P_c). Commutation losses consist of turn-on and turn-off losses of the switch. Conduction energy losses for IGBT and diode are defined in (31)-(33) [41].

$$E_{CT_loss}(k) = \int_{T_{on}(k)} V_{ce}(t).i_c(t).dt \quad (31)$$

$$V_{ce}(t) = f(i_c(k), T_j(k)) \quad (32)$$

$$E_{CD_loss}(k) = \int_{T_{on}(k)} V_D(t).i_D(t).dt \quad (33)$$

where E_{CT_loss} and E_{CD_loss} are conduction energy losses of IGBT and diode, respectively; V_{ce} is the forward saturation voltage; V_D is the threshold voltage

of the diode; i_c denotes the collector current; k is the k^{th} switching cycle; and $T_{on}(k)$ is the on-time period of devices for the k^{th} switching cycle.

The commutation energy losses of IGBT are also defined in terms of current and temperature, as in Eqs. (34) and (35).

$$E_{sw_on}(k) = f_{sw_on}(i_c(k), T_j(k)) \quad (34)$$

$$E_{sw_off}(k) = f_{sw_off}(i_c(k), T_j(k)) \quad (35)$$

where T_j is the junction operating temperature. Total commutation energy losses are given by Eq. (36).

$$E_{sw}(k) = f_{sw_on}(k) + f_{sw_off}(k) \quad (36)$$

The commutation losses of a diode based on the recovery energy (E_{rr}) are obtained by Eq. (37) [42].

$$E_{rr}(k) = f(i_c(k), T_j(k)) \quad (37)$$

Mean total commutation power losses is calculated by Eq. (38).

$$P_{sw_ave}(k) = \frac{1}{T_{sw}} E_{sw}(k) \quad (38)$$

Total power losses are calculated by the sum of conduction and commutation losses from Eq. (39).

$$P_{ave_loss}(k) = P_{sw_ave}(k) + P_{cond_ave}(k) \quad (39)$$

There are curves in the form of a graph similar to Fig. 10 in the datasheet of inverters. Using these curves, the information regarding energy losses can be extracted.

The currents of IGBT and diode are based on the on/off states of switches and are determined by Eqs. (40) and (41) [41].

$$\begin{bmatrix} i_{T1} \\ i_{T2} \\ i_{T3} \\ i_{T4} \\ i_{T5} \\ i_{T6} \end{bmatrix} = \frac{1}{2} \begin{bmatrix} (1+\text{sign})S_1 & 0 & 0 \\ 0 & (1+\text{sign})S_2 & 0 \\ 0 & 0 & (1+\text{sign})S_3 \\ (1-\text{sign})S_4 & 0 & 0 \\ 0 & (1-\text{sign})S_5 & 0 \\ 0 & 0 & (1-\text{sign})S_6 \end{bmatrix} \cdot \begin{bmatrix} i_a \\ i_b \\ i_c \end{bmatrix} \quad (40)$$

$$\begin{bmatrix} i_{D1} \\ i_{D2} \\ i_{D3} \\ i_{D4} \\ i_{D5} \\ i_{D6} \end{bmatrix} = \frac{1}{2} \begin{bmatrix} (1-\text{sign})S_1 & 0 & 0 \\ 0 & (1-\text{sign})S_2 & 0 \\ 0 & 0 & (1-\text{sign})S_3 \\ (1+\text{sign})S_4 & 0 & 0 \\ 0 & (1+\text{sign})S_5 & 0 \\ 0 & 0 & (1+\text{sign})S_6 \end{bmatrix} \cdot \begin{bmatrix} i_a \\ i_b \\ i_c \end{bmatrix} \quad (41)$$

where i denotes the switch number ($i=1, 2, \dots, 6$); D_i and T_i are the i^{th} anti-parallel diode and the i^{th} IGBT, respectively; and S_i represents the switching states of IGBT. If a switch is on, the value of S_i is 1, and if it is

off, the value of S_i is zero. The schematic diagram of currents in a three-phase inverter is presented in Fig. 11.

6. SIMULATION RESULTS

The simulation of a dual stator winding squirrel-cage induction motor drive is performed in MATLAB/Simulink to evaluate the proposed methods. The parameters of a real DSWIM are given in the Appendix [6]. The parameters of the utilized IGBT/Diode are selected from SKM40GD123D IGBT. The simulation has been run in the following three models:

1. The conventional control model of the DSWIM drive (conventional method).
2. The proposed control model of the DSWIM drive with two three-phase inverters (Proposed Method 1).
3. The proposed control model of the DSWIM drive with five-leg inverter (Proposed Method 2).

6.1. Simulation results of the conventional method

In the conventional model, either the first or the second winding is usually fed by a constant frequency source at low speeds, and the frequency of the second winding is determined based on the requested speed and torque.

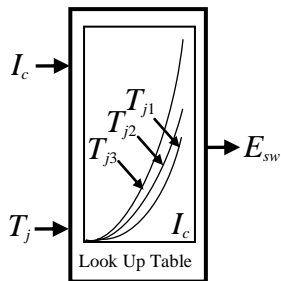


Fig. 10. Commutation energy losses of the selected IGBT.

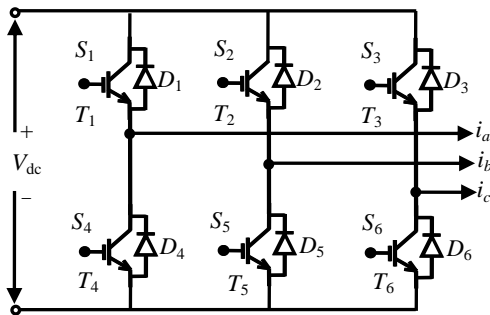


Fig. 11. A three-phase inverter circuit.

Since frequency is held constant at a minimum value in the first winding, the second winding can work in either motor or generator operating mode. In other words, the algebraic sum of the torques produced by $abc1$ and $abc2$ windings has to be equal to the requested torque. In the simulation performed for the conventional method, the excitation frequency of the first winding is held constant at a minimum value.

Figures 12 and 13 respectively demonstrate the behavior of the conventional drive control system of DSWIM in response to speed commands of (a) 4 rad/s with the torque value of 5 N.m, and (b) 0.5 rad/s with the torque value of 1 N.m. The drive control system perfectly traces low reference speeds in the steady state. Figs. 12(b) and 13(b) show the total torque (T_e) and the profile of the torque produced by $abc1$ and $abc2$ windings (T_{e1} and T_{e2}). T_e is obtained from the sum of T_{e1} and T_{e2} ($T_e=T_{e1}+T_{e2}$).

6.2. Simulation results of Proposed Method 1

Figures 14 and 15 respectively illustrate the behavior of the proposed drive control system of DSWIM, based on two three-phase inverters, in response to speed commands of (a) 4 rad/s with the torque value of 5 N.m, and (b) 0.5 rad/s with the torque value of 1 N.m.

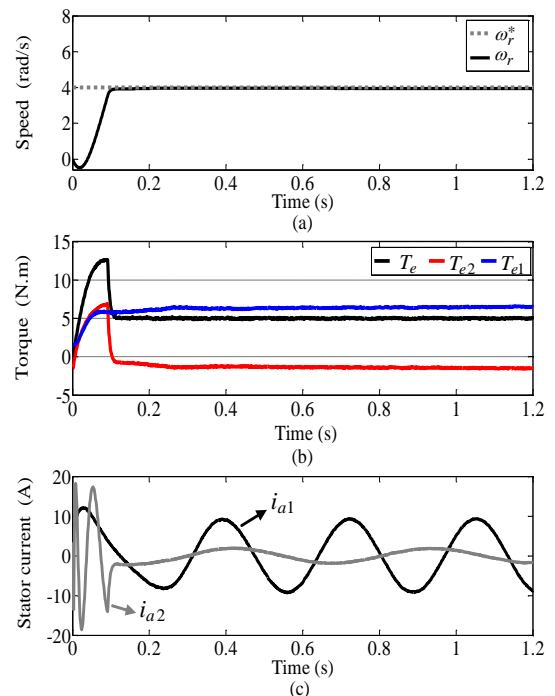


Fig. 12. Simulation results of the conventional drive control system of a DSWIM. The reference speed is 4 rad/s and the torque value is 5 N.m. a) Rotor speed profile, b) Torque profile, and c) Stator currents i_{a1} and i_{a2} .

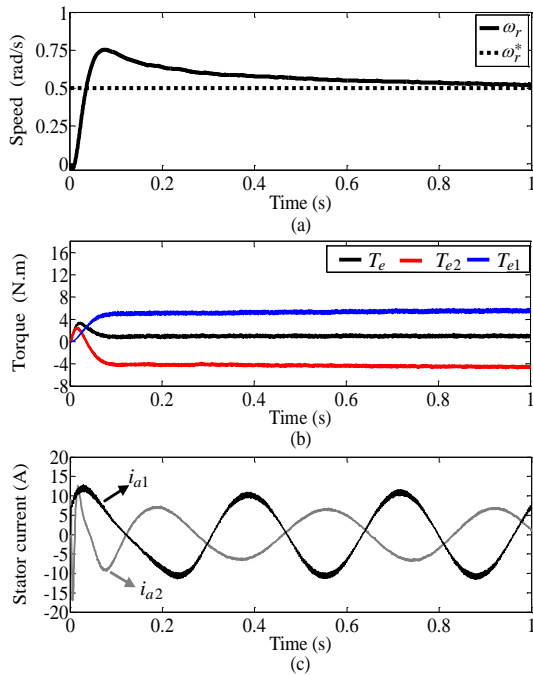


Fig. 13. Simulation results of the conventional drive control system of a DSWIM. The reference speed is 0.5 rad/s and the torque value is 1 N.m: a) Rotor speed profile, b) Torque profile, and c) Stator currents i_{a1} and i_{a2} .

The drive control system perfectly traces low reference speeds in the steady state. Figs. 14(b) and 15(b) show the total torque (T_e) and the profile of the torque produced by $abc1$ and $abc2$ windings (T_{e1} and T_{e2}). T_e is calculated from the sum of T_{e1} and T_{e2} ($T_e = T_{e1} + T_{e2}$).

Each of the torques produced by stator windings makes a percentage of the total torque, and the sum of the percentages does not exceed 100. This is an important feature of the standard operating mode of this motor.

The phase currents of $a1$ and $a2$ are shown in Figs. 14(e) and 15(e), respectively. In addition, Figs. 14(d) and 15(d) depict the estimated rotor fluxes.

6.3. Simulation results of Proposed Method 2

Figure 16 shows the behavior of the proposed drive control system of the DSWIM based on a five-leg (ten-switch) inverter, in response to the speed command of 4 rad/s with the torque value of 5 N.m. The drive control system traces this low reference speed in the steady state as perfectly as Proposed Method 1.

Figure 17 demonstrates the behavior of the proposed drive control system of the DSWIM based on a five-leg (ten-switch) inverter, in response to speed command 0.5 rad/s with the torque value of 1 N.m. The drive control system traces this very low reference speed in the steady state as perfectly as Proposed Method 1.

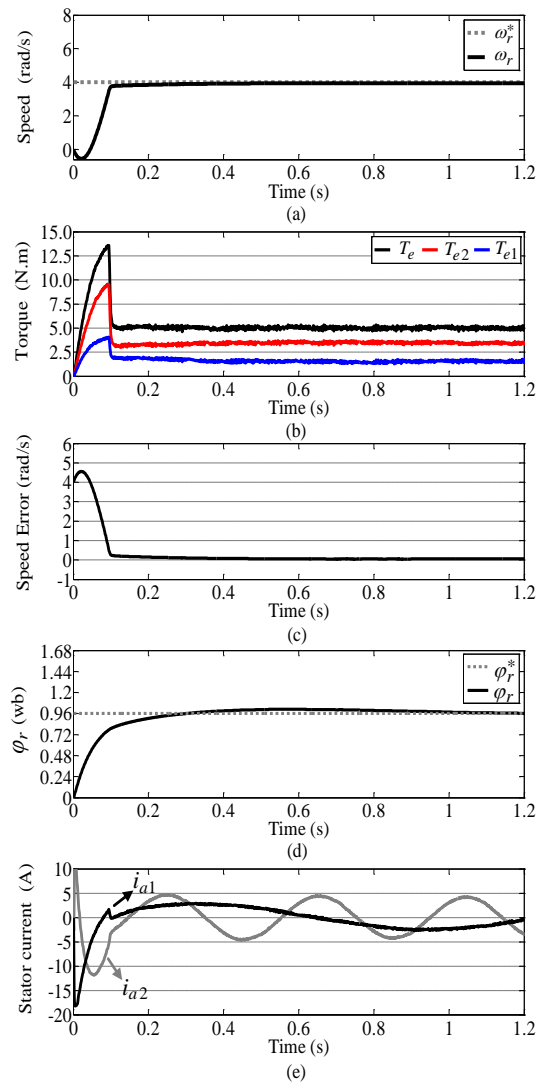


Fig. 14. Simulation results of Proposed Method 1. The reference speed is 4 rad/s and the torque value is 5 N.m. a) Rotor speed profile, b) Torque profile, c) Speed error, d) Estimated rotor flux, and e) Stator currents i_{a1} and i_{a2} .

Figures 16(b) and 17(b) show the total torque (T_e) and the profile of the torque produced by $abc1$ and $abc2$ windings (T_{e1} and T_{e2}). T_e is calculated from the sum of T_{e1} and T_{e2} . Fig. 16(e) presents the phase currents of $a1$ and $a2$. The three-phase stator currents of $abc1$ and $abc2$ windings (i_{abc1} and i_{abc2}) are demonstrated in Fig. 17(e). Figures 16(d) and 17(d) depict rotor fluxes.

6.4. Comparing the simulation results of the Proposed Methods 1 and 2 with the conventional method

A DSWIM has two three-phase stator windings. The T/I criteria is defined as the ratio of the induced torque of a DSWIM (T) per ampere. The torque per ampere ratios (T/I) produced in the DSWIM drive for both proposed methods and the conventional method are shown in Figs. 18(a) and 19(a).

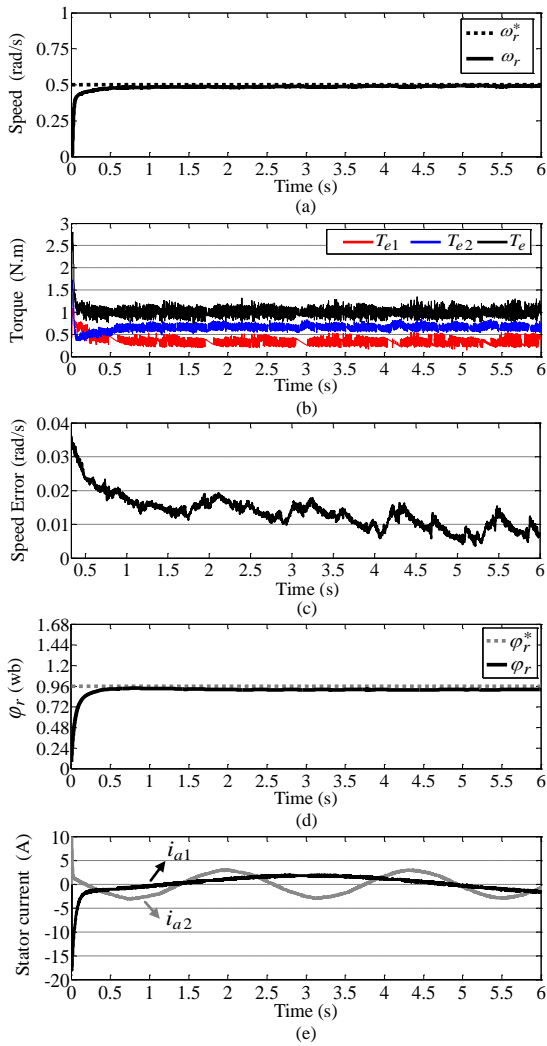


Fig. 15. Simulation results of Proposed Method 1. The reference speed is 0.5 rad/s and the torque value is 1 N.m. a) Rotor speed profile, b) Torque profile, c) Speed error, d) Estimated rotor flux, and e) Stator currents i_{a1} and i_{a2} .

In Fig. 18, reference speed is 4 rad/s and torque value is 5 N.m. In Fig. 19, reference speed is 0.5 rad/s and torque value is 1 N.m. The proposed methods have better T/I ratios compared to the conventional method. As reported in [6], in order to have an appropriate torque-per-ampere ratio in the DSWIM, the motor has to work in its standard operating mode.

Figures 18(b) and 19(b) show the sum of the total power losses (including conduction and commutation losses) of inverter units in both the proposed methods and the conventional method. Proposed Methods 1 and 2 have considerable reduction in losses compared to the conventional method.

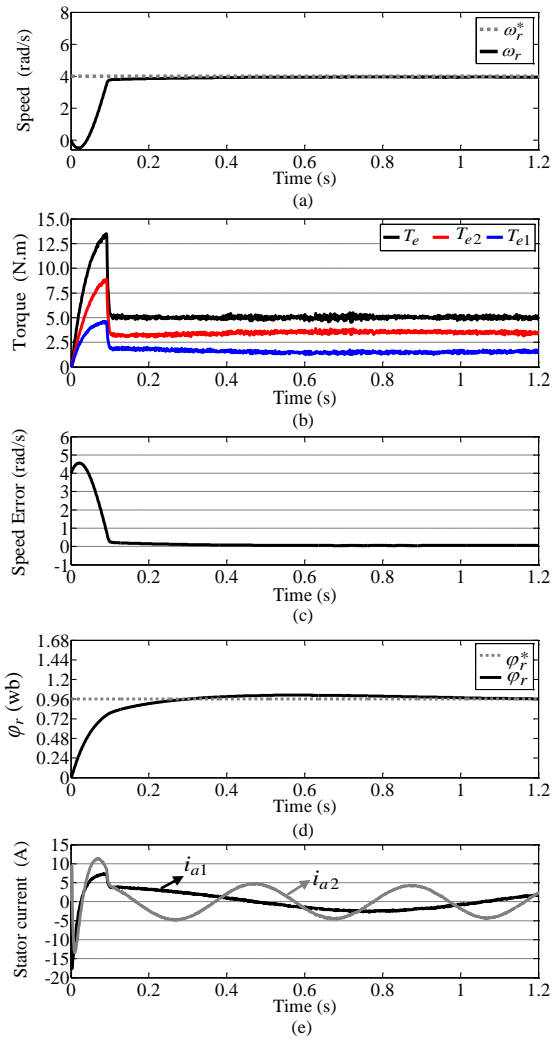


Fig. 16. Simulation results of Proposed Method 2. The reference speed is 4 rad/s and the torque value is 5 N.m. a) Rotor speed profile, b) Torque profile, c) Speed error, d) Estimated rotor flux, and e) Stator currents i_{a1} and i_{a2} .

The sum of produced torques in the proposed and conventional methods is equal to the total torque. In the conventional method, the produced torque of one of the two windings is greater than the total torque. Nevertheless, in the proposed control method, the produced torque of each winding is smaller than the total torque.

As shown in Fig. 13(b), the total torque is equal to 1 N.m, while the $abc1$ winding produces more torque than what is requested, because of its constant excitation frequency. Therefore, the high value of the torque-per-ampere ratio of the proposed methods in comparison with the conventional method is not unexpected.

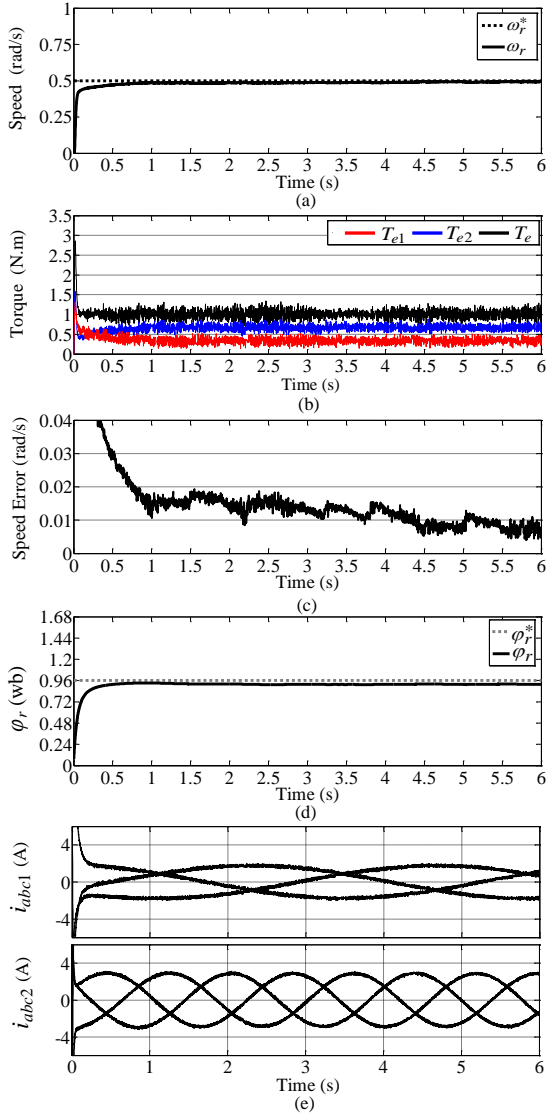


Fig. 17. Simulation results of Proposed Method 2. The reference speed is 0.5 rad/s and the torque value is 1 N.m. a) Rotor speed profile, b) Torque profile, c) Speed error, d) Estimated rotor flux, and e) Three-phase stator currents of $abc1$ and $abc2$ windings (i_{abc1} and i_{abc2}).

Figures 20 and 21 illustrate the superior performance of Proposed Methods 1 and 2 compared to the conventional method, with respect to the torque-per-ampere ratio and the reduction in the sum of total power losses (conduction and commutation losses) in the inverter unit of the DSWIM drive. In Fig. 20, reference speed is 8 rad/s and torque value is 2 N.m. In Fig. 21, reference speed is zero and torque value is 3 N.m. The sum of the absolute value of torques produced in each stator winding ($|T_{e1}|+|T_{e2}|$) is less in the proposed methods than the conventional method. Thus, the improvement in torque-per-ampere ratio and the reduction in total power losses of the inverter unit for the proposed methods compared to the conventional method is not unexpected.

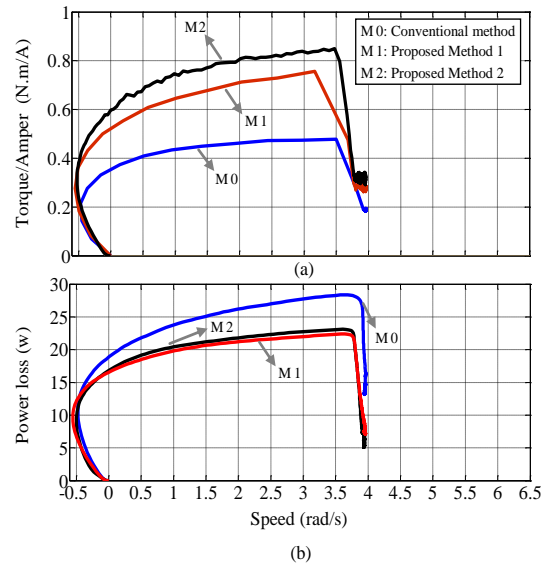


Fig. 18. Simulation results of the conventional method (M0), Proposed Method 1 (M1), and Proposed Method 2 (M2). The reference speed is 4 rad/s and the torque value is 5 N.m. a) Torque per ampere ratio, and b) Sum of the total power losses (including conduction and commutation losses) of the DSWIM drive inverter.

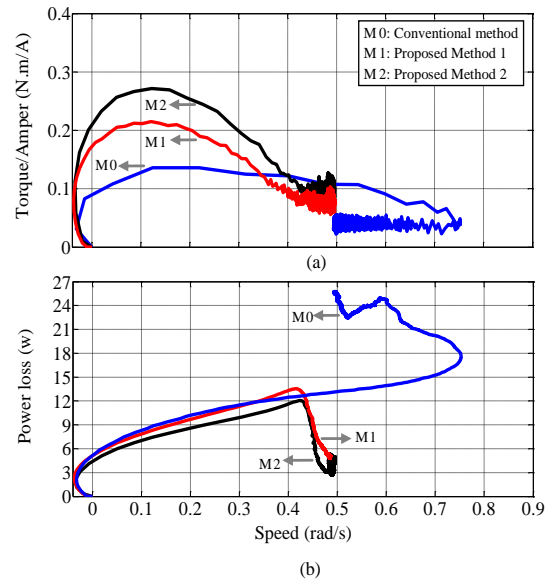


Fig. 19. Simulation results of the conventional method (M0), Proposed Method 1 (M1), and Proposed Method 2 (M2). The reference speed is 0.5 rad/s and the torque value is 1 N.m. a) Torque per ampere ratio, and b) Sum of the total power losses (including conduction and commutation losses) of the DSWIM drive inverter.

In the conventional method, the free hardware capacity of the motor, which normally includes losses, is used. Retaining the favorable performance of Proposed Method 1, Proposed Method 2 has an acceptable performance in terms of power losses of the inverter unit and reducing the costs of this unit.

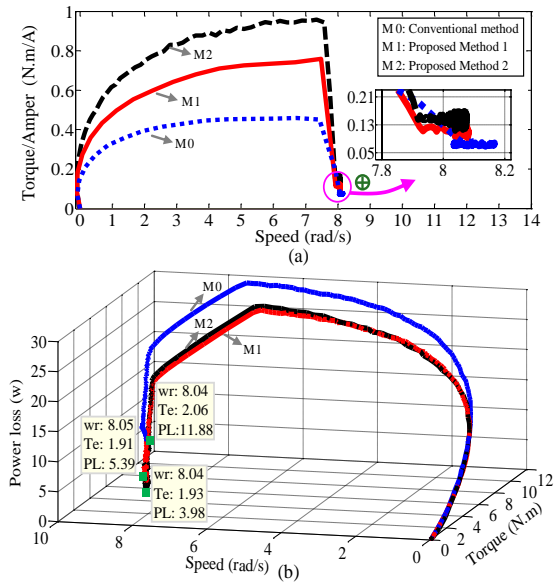


Fig. 20. Simulation results of the conventional method (M0), Proposed Method 1 (M1), and Proposed Method 2 (M2). The reference speed is 8 rad/s and the torque value is 2 N.m. a) Torque-per-ampere ratio, and b) Sum of the total power losses (including conduction and commutation losses) of the DSWIM drive inverter.

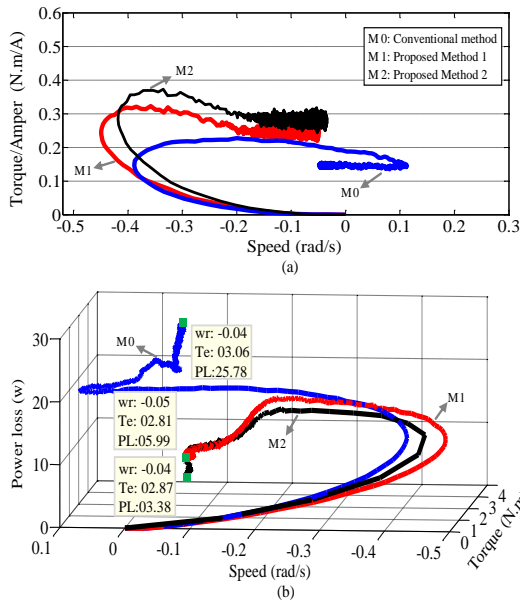


Fig. 21. Simulation results of the conventional method (M0), Proposed Method 1 (M1), and Proposed Method 2 (M2). The reference speed is zero and the torque value is 3 N.m. a) Torque-per-ampere ratio, and b) Sum of the total power losses (including conduction and commutation losses) of the DSWIM drive inverter.

An illustration of the steady-state currents of legs A, D, and C (common leg) and the corresponding spectra in the five-leg inverter of the DSWIM drive in response to the speed command of 50 rad/s and the torque value of 2 N.m is shown in Fig. 22.

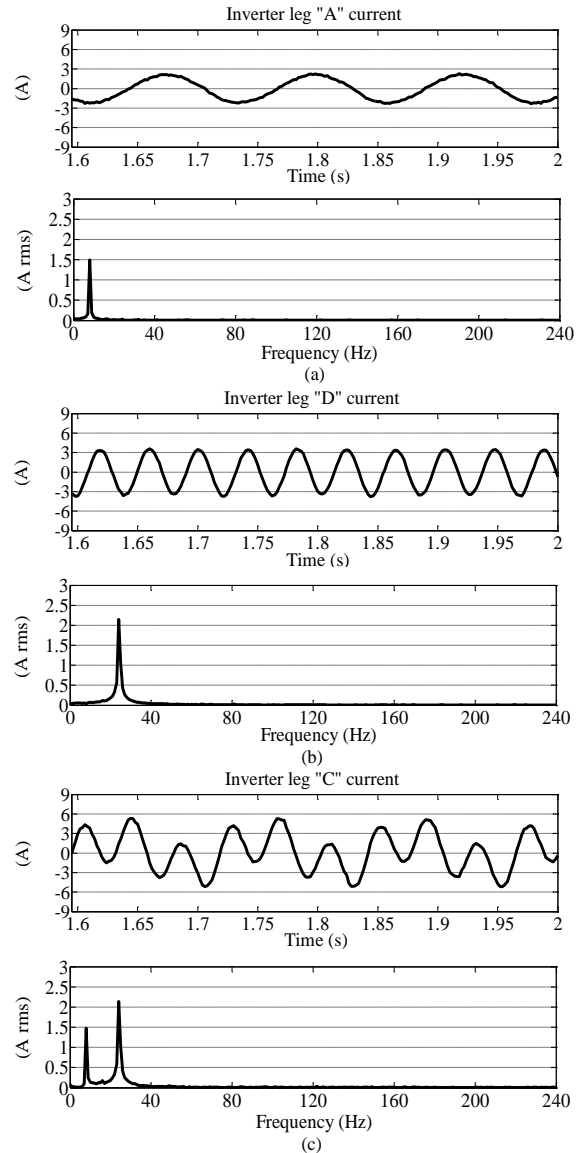


Fig. 22. Illustration of steady-state currents of legs A, D and C (common leg) and the corresponding spectra in the five-leg inverter of the DSWIM drive in response to the speed command of 50 rad/s and the torque value of 2 N.m.

The current of the common leg (C) contains two sinusoidal components at two frequencies, as can be seen from the spectrum of the current. The lower frequency belongs to i_{c1} and the higher one belongs to the third phase of the $abc2$ winding (i_{c2}). Figures 23(a) and 23(b) depicts steady-state line voltages A-C and C-D of the five-leg inverter in the DSWIM drive in response to the speed command of 50 rad/s and the torque value of 2 N.m, measured using a low-pass filter.

The voltage stress ratios of switches are presented in Fig. 23(c) according to Fig. 2. Due to symmetry, the value of the voltage stress of switches of the six-leg inverter (two three-phase inverters with the common DC-bus) is equal to the value of the voltage stress of switches of the five-leg inverter.

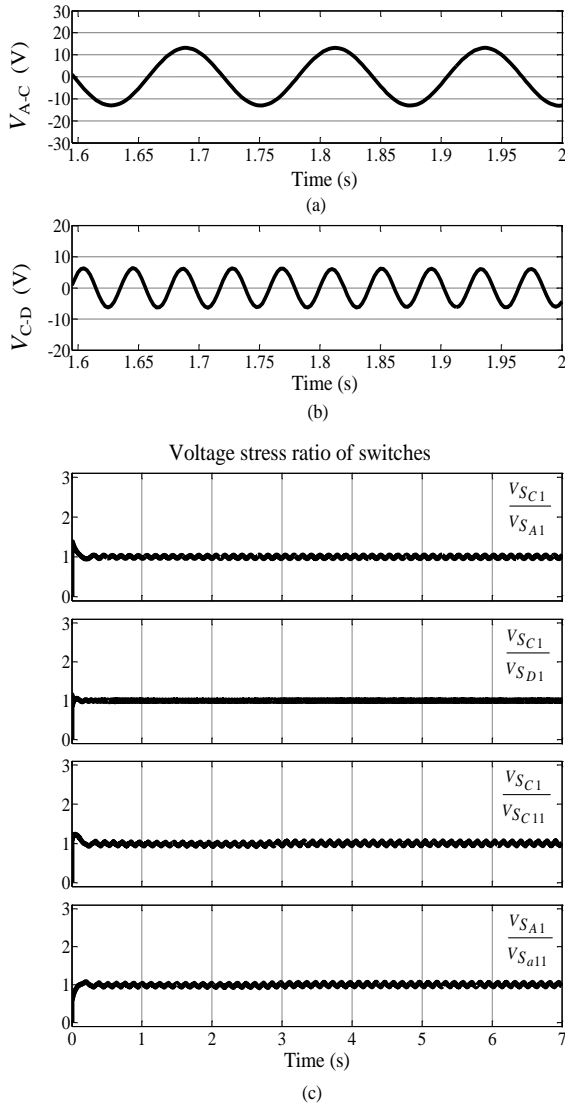


Fig. 23. The response of the DSWIM drive to the speed command of 50 rad/s and the load torque of 2 N.m a) Steady-state line voltages A-C and C-D of the five-leg inverter, and b) Voltage stress ratio of switches.

Figures 24(a), 24(b), 24(c), and 24(d) show the efficiency enhancement of the five-leg inverter compared to two three-phase inverters for different loads and speeds. In Fig. 25, the percentages of the sum of total power losses of commutation and conduction in the inverter unit of the DSWIM drive are shown in Proposed Methods 1 and 2 compared to the conventional method for speed commands of zero, 0.5, 4, and 8 rad/s with torque values of 3, 1, 5, and 2 N.m, respectively.

Reducing the number of inverter switches from 12 to 10 not only causes cost reduction but also brings about a relative success in terms of reduction in the sum of total power losses (conduction and commutation losses) of the inverter unit, as can be seen in Fig. 25.

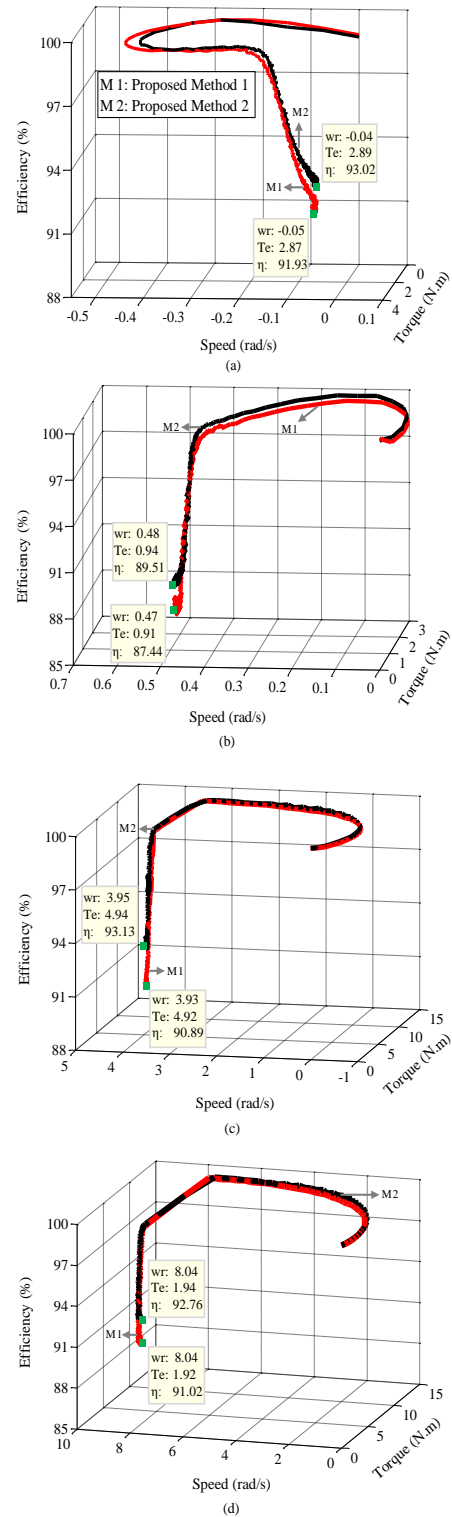


Fig. 24. Illustration of the efficiency (η) of the five-leg inverter and two three-phase inverters for different loads and speeds.

7. CONCLUSIONS

The main purpose of this paper was to present a method based on rotor flux compensation for reducing the power losses of the inverter unit in the squirrel-cage dual stator induction motor drive with dissimilar

numbers of pole at low speeds. At the standard operating mode of this motor, the two rotating fields produced by two stator windings rotate synchronously. However, in the conventional control method of the DSWIM drive at low speeds, by exciting one of the windings with a constant frequency, these two fields rotate asynchronously, and the motor does not work in its standard operating mode.

Using the idea of compensation in the proposed drive control system in DSWIM, the problem of flux estimation at low speeds was solved and the motor had a desired performance in its standard operating mode at low speeds. In this paper, the following two proposed topics were taken into account:

1. A technique was presented for rotor flux compensation in the drive control system of DSWIM that solved the problem of correct flux estimation at low speeds and reduced power losses in the inverter unit (Proposed Method 1).
2. The inverter unit of the DSWIM drive has 12 switches in total. Utilization of a five-leg (ten-switch) inverter for controlling two independent induction motors had already been investigated by researchers. In the present paper, Proposed Method 1 was investigated using this inverter. The important feature of this inverter was a reduction in the number of power electronic switches, which relatively reduced the sum of total power losses of commutation and conduction of the inverter unit (Proposed Method 2).

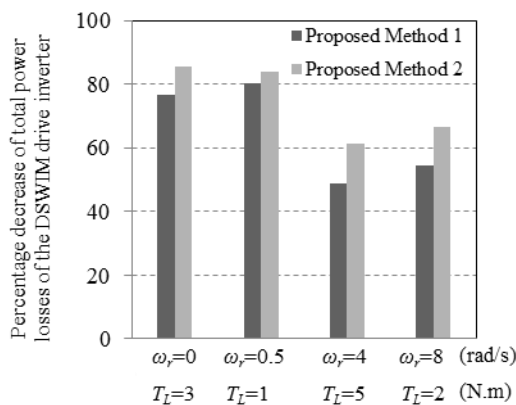


Fig. 25. Decrease in the total power losses (including conduction and commutation losses in %) of the DSWIM drive inverter in Proposed Methods 1 and 2 compared to the conventional method for speed commands of zero, 0.5, 4, and 8 rad/s with the torque values of 3, 1, 5, and 2 N.m, respectively.

Proposed Methods 1 and 2 had better torque-per-ampere ratios and power losses of the inverter unit compared to the conventional method. Simulation results confirmed the superior performance of the proposed DSWIM drives at a low speeds.

APPENDIX

Parameters of the dual stator winding squirrel-cage induction motor (DSWIM)

| Nominal power | 2 hp | $P_1:P_2$ | 2:6 |
|---------------|---------------|-----------|---------------|
| R_{s1} | 3.4 Ω | R_{s2} | 1.9 Ω |
| L_{ls1} | 0.006 H | L_{ls2} | 0.009 H |
| R_{r1} | 0.61 Ω | R_{r2} | 0.55 Ω |
| L_{lr1} | 0.006 H | L_{lr2} | 0.009 H |
| L_{m1} | 0.336 H | L_{m2} | 0.093 H |
| K_1 | 0.333 | K_2 | 0.6 |
| f_n | 60 Hz | - | - |

REFERENCES

- [1] G. K. Singh, "Multi-phase induction machine drive research-a survey," *Electr. Power Syst. Res.*, vol. 61, no. 2, pp. 139-147, 2002.
- [2] M. Bigdeli, D. Azizian, and E. Rahimpour, "An improved big bang-big crunch algorithm for estimating," *J. Oper. Autom. Power Eng.*, vol. 4, no. 1, pp. 83-92, 2016.
- [3] E. Abdi, M. R. Tatlow, R. A. McMahon, and P. J. Tavner, "Design and performance analysis of a 6 MW medium-speed brushless DFIG," in *Proce. of the Renewable Power Gener. Conf.*, 2013, pp. 1-4.
- [4] P. C. Roberts, "A study of brushless doubly-fed (induction) machines," *PhD dissertation, Dept. Eng., Univ. Cambridge*, 2005.
- [5] A. R. Muñoz and T. A. Lipo, "Dual stator winding induction machine drive," *IEEE Trans. Ind. Appl.*, vol. 36, no. 5, pp. 1369-1379, 2000.
- [6] J. M. Guerrero and O. Ojo, "Total airgap flux minimization in dual stator winding induction machines," *IEEE Trans. Power Electr.*, vol. 24, no. 3, pp. 787-795, Mar. 2009.
- [7] R. Ueda, T. Sonoda, M. Ichikawa, and K. Koga, "Stability analysis in induction motor driven by V/f controlled general purpose inverter," *IEEE Trans. Ind. Appl.*, vol. 82, no. 2, pp. 472-481, 1992.
- [8] R. Bojoi, F. Farina, G. Griva, and F. Profumo, "Direct torque control for dual three-phase motor drives," *IEEE Trans. Ind. Appl.*, vol. 41, no. 6, pp. 1627-1636, 2005.
- [9] K. Pienkowski, "Analysis and control of dual stator winding induction motor," *Archi. Electr. Eng.*, vol. 61, no. 3, pp. 421-438, 2012.
- [10] S. Basak, and C. Chakraborty, "Dual stator winding induction machine: problems, progress and future scope," *IEEE Trans. Ind. Electron.*, vol. 62, no. 7, pp. 4641-4652, 2015.

- [11] Z. Wu, O. Ojo, and J. Sastry, "High-performance control of a dual stator winding DC power induction generator," *IEEE Trans. Ind. Appl.*, vol. 43, no. 2, pp. 582-592, 2007.
- [12] O. Ojo and Z. Wu, "Speed control of a dual stator winding induction machine," in *Proc. Of the IEEE Applied Power Electronics Conference*, 2007, pp. 229-235.
- [13] M. B. Slimene, M. L. Khelifi, M. B. Fredj, and H. Rehaouia, "Indirect field-oriented control for dual stator induction motor drive," *Proc. Of the 10th Int. Multi-Conf. Syst., Signals Devices*, pp. 18-21, 2013.
- [14] H. Moayedirad, M. A. Shamsinejad, and M. Farshad, "Neural control of the induction motor drive: robust against rotor and stator resistances variations and suitable for very Low and high speeds," *Iran J. Elect. Com. Eng.*, vol. 9, no. 2, pp 107-113, 2011.
- [15] H. Moayedirad, M. Farshad, and M.A. Shamsinejad, "Improvement of speed profile in induction motor drive using a new idea of PWM pulses generation base on artificial neural networks," *Inte. Syst. Electr. Eng.*, vol. 2, no. 4, pp 35-46, 2012.
- [16] H. Moayedirad, M. A. Shamsinejad, and M. Farshad, "Improvement of induction motor drive operation in low and high speeds using rotor flux compensation," *J. Iran Association. Electr. & Electron. Eng.*, vol. 9, no. 2, pp. 59-64, 2012.
- [17] D. G. Holmes, B. P. McGrath, and S. G. Parker, "Current regulation strategies for vector-controlled induction motor drives," *IEEE Trans. Ind. Electro.*, vol. 59, no. 10, pp. 3680-3689, 2012.
- [18] B. M. Joshi and M. C. Chandorkar, "Vector control of two-motor single-inverter induction machine drives," *Electr. Power Compo. Syst.*, vol. 42, no. 11, pp. 1158-1171, 2014.
- [19] R. D. Lorenz and D. B. Lawson, "A simplified approach to continuous on-line tuning of field oriented induction motor drives," *IEEE Trans. Ind. Appl.*, vol. 26, no. 3, pp. 420-424, 1990.
- [20] M. P. Kazmierkowski, "A novel vector control scheme for transistor PWM inverter-fed induction motor drive," *IEEE Trans. Ind. Appl.*, vol. 38, no. 1, pp. 41-47, 1991.
- [21] H. M. Kojabadi, L. Chang, and R. Doraiswami, "A MRAS-based adaptive pseudoreduced-order flux observer for sensorless induction motor drives," *IEEE Trans. Power Electron.*, vol. 20, no. 4, pp. 930-176, 2005.
- [22] M. S. Zaky and M. K. Metwaly, "Sensorless torque/speed control of induction motor drives at zero and low frequencies with stator and rotor resistance estimations," *IEEE J. Emerg. and Sel. Top. Power Electr.*, vol. 4, no. 4, pp. 1416-1429, 2016.
- [23] C. P. Salomon et al., "Induction motor efficiency evaluation using a new concept of stator resistance," *IEEE Trans. Instrum. Meas.*, vol. 64, no. 11, pp. 2908-2917, 2015.
- [24] J. Chen and J. Huang, "Online decoupled stator and rotor resistances adaptation for speed sensorless induction motor drives by a time-division approach," *IEEE Trans. Power Electr.*, vol. 32, no. 6, pp. 4587-4599, 2017.
- [25] A. Dey, B. Singh, B. Dwivedi, and D. Chandra, "Vector control of three-phase induction motor using artificial intelligent technique," *ARNP J. Eng. and Appl. Sci.*, vol. 4, no. 4, pp. 57-67, 2009.
- [26] Z. G. Yin, C. Zhao, and Y. R. Zhong, "Research on robust performance of speed-sensorless vector control for the induction motor Using an interfacing multiple-model extended kalman filter," *IEEE Trans. Power Electr.*, vol. 29, no. 6, pp. 3011 - 3019, 2014.
- [27] I. M. Alsofyani and N. R. N. Idris, "Simple flux regulation for improving state estimation at very low and zero speed of a speed sensorless direct torque control of an induction motor," *IEEE Trans. Power Electr.*, vol. 31, no. 4, pp. 3027- 3035, 2016.
- [28] I. M. Alsofyani and N. R. N. Idris, "Lookup-table-based DTC of induction machines with improved flux regulation and extended kalman filter state estimator at low-speed operation," *IEEE Trans. Ind. Inform.*, vol. 12, no. 4, pp. 1412-1425, 2016.
- [29] D. Stojic, M. Milinkovic, S. Veinovic, and I. Klasnic, "Improved stator flux estimator for speed sensorless induction motor drives," *IEEE Trans. Power Electr.*, vol. 30, no. 4, pp. 2363 - 2371, 2015.
- [30] M. Jones, S. N. Vukosavic, D. Dujic, E. Levi, and P. Wright, "Five-leg inverter PWM technique for reduced switch count two-motor constant power applications," *IET Electr. Power Appl.*, vol. 2, no. 5, pp. 275-287, 2008.
- [31] S. Laali, E. Babaei, and M. B. B. Sharifian, "Reduction the number of power electronic devices of a cascaded multilevel inverter based on new general topology," *J. Oper. Autom. Power Eng.*, vol. 2, no. 2, pp. 81-90, 2014.
- [32] K. Oka, Y. Nozawa, and K. Matsuse, "An improved method of voltage utility factor for PWM control of a five-leg inverter in two induction motor drives," *IEEE Trans. Electr. and Electron. Eng.*, vol. 1, no. 1, pp. 108-111, 2006.
- [33] C. S. Lim, N. A. Rahim, W. P. Hew, and E. Levi, "Model predictive control of a two-motor drive with five-leg-inverter supply," *IEEE Trans. Ind. Electr.*, vol. 60, no. 1, pp. 54-65, 2013.
- [34] Y. Mei and S. Feng, "An optimized modulation method for a five-leg-inverter for dual induction motor drives," in *Proce. of the IPEMC-ECOC*, 2016, pp. 660-663.
- [35] S. Dangeam and V. Kinnarees, "Five-leg voltage source inverter for driving two single-phase induction motors," in *Proce. of the 17th Int. Conf. Electr. Mach. Syst.*, 2014, pp. 156 - 161.
- [36] O. Ojo and Z. Wu, "Modeling of a dual-stator-winding induction machine including the effect of main flux linkage magnetic saturation," *IEEE Trans. Ind. Appl.*, vol. 44, no. 4, pp. 1099-1107, 2008.
- [37] B. K. Bose, *Modern Power Electronics and AC Drives*. Upper Saddle River, NJ: Prentice-Hall, 2002.
- [38] J. Hu and B. Wu, "New integration algorithms for estimating motor flux over a wide speed range," *IEEE Trans. Power Electr.*, vol. 13, no. 5, pp.969-976, 1998.
- [39] E. Babaei, M. H. Babayi, E. ShokatiAsl, and S. Laali, "A new topology for Z-source inverter based on switched-inductor and boost Z-source inverter," *J. Oper. Autom. Power Eng.*, vol. 3, no. 2, pp. 167-184, 2015.
- [40] D. W. Novotny and T. A. Lipo, *Vector Control and Dynamics of AC Drives*. Oxford University Press, 1997.
- [41] Z. Zhou, M. S. Khanniche, P. Igc, S. M. Towers, and P. A. Mawby, "Power loss calculation and thermal modelling for a three phase inverter drive system," *J. Electri. Syst.*, vol. 1, no. 4, pp.33-46, 2005.
- [42] J. Pou, D. Osorno, J. Zaragoza, S. Ceballos, and C. Jaen, "Power losses calculation methodology to evaluate

inverter efficiency in electrical vehicles,” in *Proce. of the 17th Int. Conf. Work. Compab. Power. Electron.*, 2011, pp. 400-409.